Article

Cell Reports

Genome-wide CRISPR-Cas9 Screens Reveal Loss of Redundancy between PKMYT1 and WEE1 in Glioblastoma Stem-like Cells

Graphical Abstract

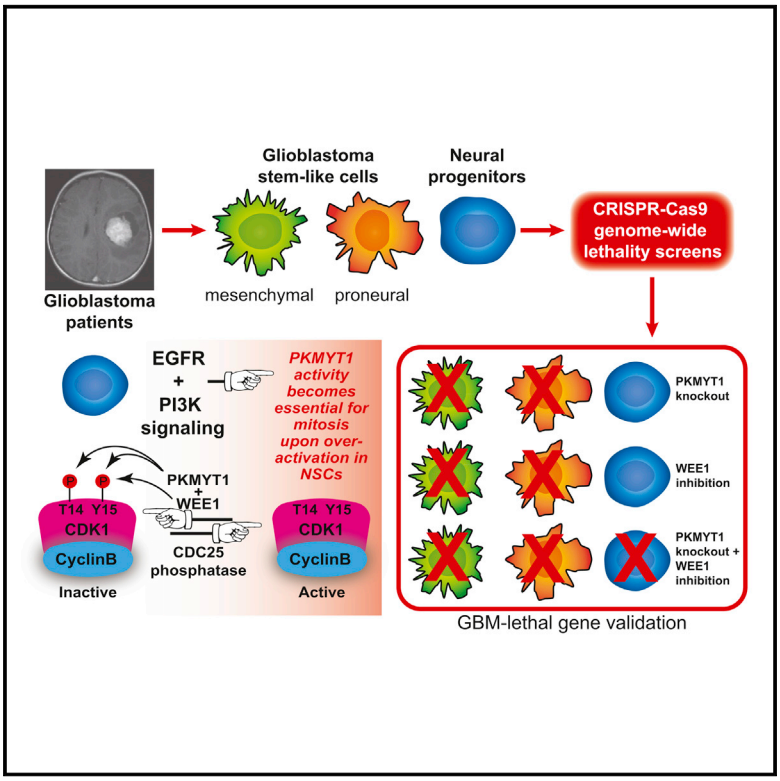

Authors

Chad M. Toledo, Yu Ding, Pia Hoellerbauer, ..., Bruce E. Clurman, James M. Olson, Patrick J. Paddison

Correspondence

jolson@fredhutch.org (J.M.O.), paddison@fredhutch.org (P.J.P.)

In Brief

Patient-derived glioblastoma stem-like cells (GSCs) can be grown in conditions that preserve patient tumor signatures and their tumor initiating capacity. Toledo et al. use these conditions to perform genome-wide CRISPR-Cas9 lethality screens in both GSCs and non-transformed NSCs, revealing PKMYT1 as a candidate GSC-lethal gene.

Highlights

- CRISPR-Cas9 lethality screens performed in patient brain-tumor stem-like cells
- PKMYT1 is identified in GSCs, but not NSCs, as essential for facilitating mitosis
- PKMYT1 and WEE1 act redundantly in NSCs, where their inhibition is synthetic lethal
- PKMYT1 and WEE1 redundancy can be broken by over-activation of EGFR and AKT

Toledo et al., 2015, Cell Reports *13*, 2425–2439
December 22, 2015 ©2015 The Authors
http://dx.doi.org/10.1016/j.celrep.2015.11.021

Cell Reports
Article

Genome-wide CRISPR-Cas9 Screens Reveal Loss of Redundancy between PKMYT1 and WEE1 in Glioblastoma Stem-like Cells

Chad M. Toledo,[1,2,14] Yu Ding,[1,14] Pia Hoellerbauer,[1,2] Ryan J. Davis,[1,2,3] Ryan Basom,[4] Emily J. Girard,[3] Eunjee Lee,[5] Philip Corrin,[1] Traver Hart,[6,7] Hamid Bolouri,[1] Jerry Davison,[4] Qing Zhang,[4] Justin Hardcastle,[1] Bruce J. Aronow,[8] Christopher L. Plaisier,[9] Nitin S. Baliga,[9] Jason Moffat,[6,7] Qi Lin,[10] Xiao-Nan Li,[10] Do-Hyun Nam,[11] Jeongwu Lee,[12] Steven M. Pollard,[13] Jun Zhu,[5] Jeffery J. Delrow,[4] Bruce E. Clurman,[1,3] James M. Olson,[3,*] and Patrick J. Paddison[1,2,*]
[1]Human Biology Division, Fred Hutchinson Cancer Research Center, Seattle, WA 98109, USA
[2]Molecular and Cellular Biology Program, University of Washington, Seattle, WA 98195, USA
[3]Clinical Research Division, Fred Hutchinson Cancer Research Center, Seattle, WA 98109, USA
[4]Genomics and Bioinformatics Shared Resources, Fred Hutchinson Cancer Research Center, Seattle, WA 98109, USA
[5]Department of Genetics and Genomic Sciences, Icahn Institute of Genomics and Multiscale Biology, Icahn School of Medicine at Mount Sinai, New York, NY 10029, USA
[6]Department of Molecular Genetics, University of Toronto and Donnelly Centre, Toronto, ON M5S3E1, Canada
[7]Canadian Institute for Advanced Research, Toronto, ON M5G1Z8, Canada
[8]Division of Biomedical Informatics, Cincinnati Children's Hospital Medical Center, Cincinnati, OH 45229, USA
[9]Institute for Systems Biology, Seattle, WA 98109, USA
[10]Brain Tumor Program, Texas Children's Cancer Center, Department of Pediatrics, Baylor College of Medicine, Houston, TX 77030, USA
[11]Institute for Refractory Cancer Research, Samsung Medical Center, Seoul 135-710, Korea
[12]Department of Stem Cell Biology and Regenerative Medicine, Lerner Research Institute, Cleveland Clinic, Cleveland, OH 44192, USA
[13]Edinburgh CRUK Cancer Research Centre and MRC Centre for Regenerative Medicine, The University of Edinburgh, Edinburgh EH16 4UU, UK
[14]Co-first author
*Correspondence: jolson@fredhutch.org (J.M.O.), paddison@fredhutch.org (P.J.P.)
http://dx.doi.org/10.1016/j.celrep.2015.11.021

SUMMARY

To identify therapeutic targets for glioblastoma (GBM), we performed genome-wide CRISPR-Cas9 knockout (KO) screens in patient-derived GBM stem-like cells (GSCs) and human neural stem/progenitors (NSCs), non-neoplastic stem cell controls, for genes required for their in vitro growth. Surprisingly, the vast majority GSC-lethal hits were found outside of molecular networks commonly altered in GBM and GSCs (e.g., oncogenic drivers). In vitro and in vivo validation of GSC-specific targets revealed several strong hits, including the wee1-like kinase, *PKMYT1/Myt1*. Mechanistic studies demonstrated that PKMYT1 acts redundantly with WEE1 to inhibit cyclin B-CDK1 activity via CDK1-Y15 phosphorylation and to promote timely completion of mitosis in NSCs. However, in GSCs, this redundancy is lost, most likely as a result of oncogenic signaling, causing GBM-specific lethality.

INTRODUCTION

One popular concept in cancer research is the notion that genomic and molecular profiling of patient samples will enable the discovery of patient-tailored therapeutic strategies. However, it remains unclear whether analytic or computational approaches based solely on descriptive datasets are powerful enough to predict successful therapies. An alternative approach is to directly identify molecular vulnerabilities in patient samples using functional genetic experimentation. This has recently been achieved for glioblastoma (GBM) (Chudnovsky et al., 2014; Ding et al., 2013; Gargiulo et al., 2013; Goidts et al., 2012; Hubert et al., 2013; Kitambi et al., 2014; Toledo et al., 2014; Wurdak et al., 2010), the most aggressive and common form of brain cancer in adults (American Cancer Society, 2010; Stupp et al., 2005).

Loss of gene function RNAi screens have been performed directly in patient-derived GBM stem-like cells (GSCs) for candidate therapeutic targets and GBM regulatory networks (Chudnovsky et al., 2014; Ding et al., 2013; Gargiulo et al., 2013; Goidts et al., 2012; Hubert et al., 2013; Toledo et al., 2014; Wurdak et al., 2010). GSCs retain tumor-initiating potential and tumor-specific genetic and epigenetic signatures in vitro (Lee et al., 2006; Pollard et al., 2009), under culture conditions that mimic the neural progenitor perivascular niche (Kazanis et al., 2010; Lathia et al., 2012). By performing control screens in fetal neural stem cells (NSCs), which have similar expression profiles and developmental potential but are not transformed (Lee et al., 2006; Pollard et al., 2009), candidate GSC-specific therapeutic targets can be identified (Ding et al., 2013; Hubert et al., 2013; Toledo et al., 2014).

With the emergence of CRISPR-Cas9 gene editing technology, functional genetic single-guide RNA (sgRNA) libraries now exist that are in theory capable of triggering biallelic insertion-deletion (indel) mutations in most genes in the human genome (Shalem et al., 2014; Wang et al., 2014). In contrast to gene knockdown, these indels can cause knockout (KO)-like mutations that result in frameshifts in target genes leading to premature stop codons, non-sense mediated mRNA decay, and complete loss of protein function (Mali et al., 2013; Wiedenheft et al., 2012). However, this technology may present unique challenges for studying essential genes in mammals. For example, if Cas9 cuts are repaired by the non-homologous end-joining pathway in a non-biased manner, one-third of the time a small in-frame indel would be generated that might have little effect on protein activity.

Here, we applied a genome-wide CRISPR-Cas9 library to GSCs and NSCs in an attempt to further identify GBM candidate therapeutic targets, which when KO'd are essential to GSCs but non-essential in NSCs, suggestive of a large therapeutic window. The results from these screens provide evidence for both "individual" GSC-specific KO hits, which are found only in individual patient samples, and "convergent" KO hits, which are shared hits between GBM-isolates of different developmental subtypes and genetic alterations. Follow-up studies were focused on a strongly scoring "convergent" screen hit, *PKMYT1/Myt1* (Booher et al., 1997; Liu et al., 1997). We find that PKMYT1 and WEE1 are redundant and synthetic lethal in NSCs, where they redundantly phosphorylate CDK1-Y15 and block premature entry into mitosis. However, this redundancy is broken in GSCs or NSCs overexpressing activated alleles of EGFR and AKT1, which results in the essential requirement for PKMYT1 and timely completion of mitosis. Further, we also demonstrate that repair of CRISPR-Cas9-triggered indels exhibit frameshift bias, causing more out-of-frame indels than expected by chance, which explains the effectiveness of this technology. Our results suggest that PKMYT1 is a candidate therapeutic target for GBM. More generally, our results illustrate the utility of performing CRISPR-Cas9 screens for essential genes in patient tumor samples.

RESULTS

Genome-wide CRISPR-Cas9 Screens in Human GSCs and NSCs

We first examined the efficacy of delivering a CRISPR-Cas9 targeting system by lentiviral (LV) transduction in human GSC and NSC isolates. Consistent with previous reports, an all-in-one LV-sgRNA:Cas9 platform system was highly effective at targeting reporter and endogenous genes in both GSCs and NSCs (Figures 1A–1D), including randomly integrated copies of *EGFP* (>85%), a non-essential endogenous gene, *TP53*, assayed by western blot, and an essential gene, *MCM2* (O'Donnell et al., 2013), assayed by viability of in vitro expanded cells. In each case, we were able to observe profound reduction in target gene activity in GSCs and NSCs. Importantly, peak suppression occurred 10–14 days post-selection and non-targeting sgRNA controls had no effect on cell viability (Figure 1).

We next performed genome-wide screens using two adult GSC isolates, 0131 and 0827 (Son et al., 2009), and two control NSC lines, CB660 and U5 (Figure 2A). These GSC isolates best resemble mesenchymal and proneural GBM subtypes, respectively (Figure S2), two subtypes accounting for over half of adult GBM cases (Verhaak et al., 2010). These isolates harbor characteristic gene and pathway alterations commonly observed in GBM tumors (Brennan et al., 2013), including alterations in *EGFR*, *NF1*, *MDM2/4*, *PI3KCA*, *PTEN*, *RB1*, *TERT*, and/or *TP53* (Figures 2A and S1A–S1D; Table S1). Importantly, we did not find growth defects in NSCs or GSCs when Cas9 was stably expressed for over 3 weeks (Figure S1E).

The screens were performed using a "shot gun" approach where GSCs and NSCs were transduced with a LV pool containing a human CRISPR-Cas9 library composed of 64,751 unique sgRNAs targeting 18,080 genes (Shalem et al., 2014) and outgrown in self-renewal conditions for ~3 weeks (day 21 for NSC-U5 or day 23 for all others) (Supplemental Experimental Procedures) using two biological replicates per isolate. For the primary screen readout, we deep sequenced library sgRNAs from transduced cell populations before and after outgrowth. Based on normalized read counts, we identified 99.8% of all sgRNAs in the library pool. Each screen replicate tightly clustered at day 0 but displayed cell-type-specific differences after expansion (Figure 2B). Importantly, sgRNA sequence reads were well correlated between biological replicates with Pearson's r values of 0.98 for all day 0 replicates and $\geq$0.79 for ~3-week-outgrown replicates (Figure S2A).

To assess changes in individual sgRNA representation, edgeR (empirical analysis of digital gene expression in R) was used (Robinson et al., 2010) (Supplemental Experimental Procedures). While edgeR has been mainly used for examining changes in steady-state mRNA levels from SAGE and RNA sequencing (RNA-seq) data, by design, edgeR was intended for use with any type of count based sequence tag data in complex libraries, including nucleic acid bar codes (Dai et al., 2014). To do so, edgeR models the count variance across replicates as a nonlinear function of the mean counts using a negative binomial distribution while accounting for over all data dispersion. The output of edgeR provides fold changes for each individual sgRNA's sequenced reads, in our case, between day 21 or 23 and day 0 and also provides a statistical test similar to a Fisher's exact test to determine significance. This approach revealed thousands of significantly scoring sgRNAs for each screen at day 21 or 23, representing both candidate essential and growth limiting genes (Figure 2C; Table S2).

To assess screen and edgeR performance, we employed a Bayesian classifier that uses predetermined essential and non-essential gene training sets to help determine functional genetic screen quality (Hart et al., 2014) (Figures S2B–S2D; Table S3). This analysis allowed independent scoring of essential genes in each isolate, supporting observations reported below for edgeR analysis (Figure S2E).

Further, given that CRISPR-Cas9 technology relies on nuclease cleavage of target sites, there is the possibility that copy-number variation (CNV) in target sites could affect screen outcome. Using hypergeometric testing, we did not observe

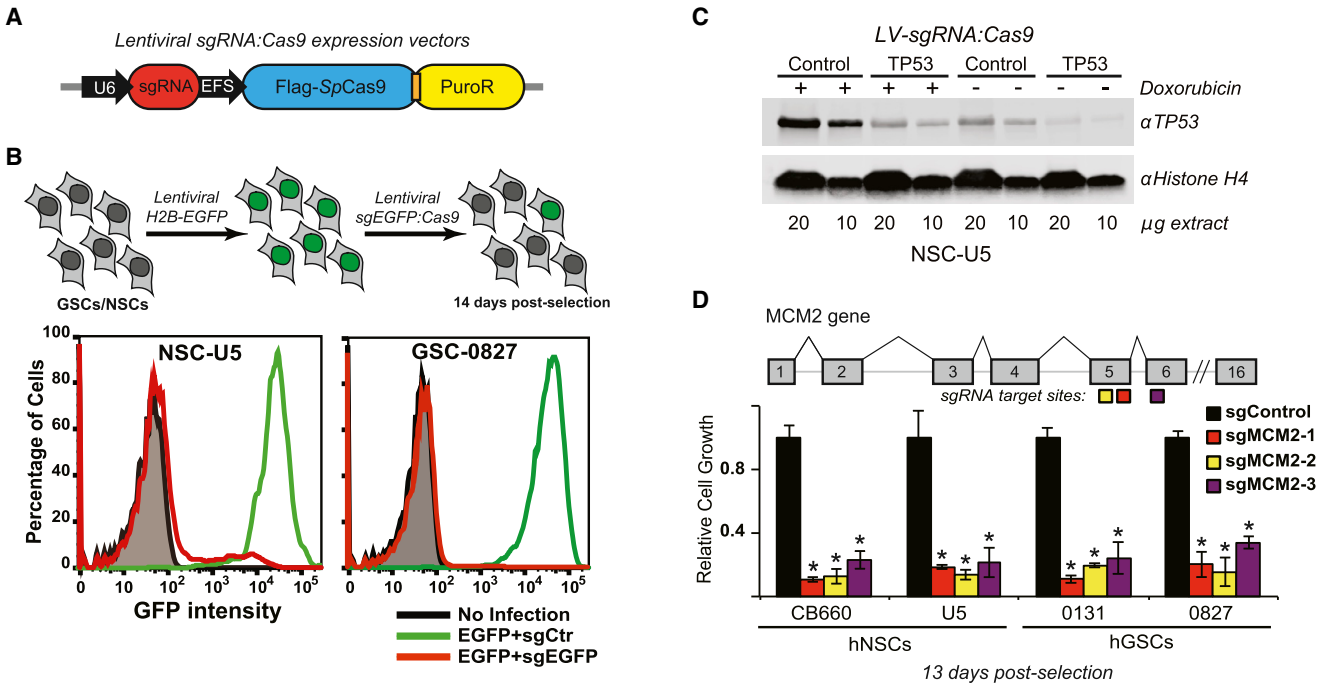

Figure 1. Validation of CRISPR-Cas9-Based Gene Targeting in Human GSCs and NSCs

(A) Cartoon of lentiviral construct used for sgRNA:Cas9 expression.

(B) sgEGFP:Cas9 was used to target stably expressed H2B-EGFP in GSCs and NSCs. Cells were first infected with LV-EGFP-H2B at MOI >2 and passaged for 1 week and then infected with sgControl or sgEGFP at MOI <1, selected, outgrown for 14 days, and flow analyzed. Similar results were obtained for each NSC-CB660s and GSC-0131s (data not shown). At day 5 post-selection, for $EGFP^{+}$sgEGFP NSC-CB660s, we noted 19.5% of cells still positive for GFP, while by D12, this number was reduced to <1%, suggesting that peak suppression probably occurs around D10 for a single, mono-allelic genomic target. However, a small percentage of wild-type (non-edited) cells remained at D12 post-selection after targeting the endogenous gene CREBBP (Figure 7), and, thus, the peak suppression occurs between D10 and D14 depending on the target.

(C) Western blot confirmation of TP53 protein expression after targeting TP53 gene with sgRNA:Cas9 in NSC-U5s. Cells were outgrown for >21 days following selection. Doxorubicin treatment (0.75 μg/ml for 6 hr) was used to stabilize TP53 in response to DNA damage.

(D) CRISPR-Cas9-based targeting of an essential gene, MCM2. Cells were infected with sgRNAs and seeded 3 days post-selection for a 10-day culture in triplicate. Cell viability was then measured using alamarBlue reagent. *$p < 0.01$, Student's t test (unpaired, unequal variance).

enrichment of GSC screen hits at specific genome addresses, nor did we observe enrichment for genes contained within sites of GSC-specific CNV among screen hits (data not shown). This suggests that CNV differences in GSCs were not a major factor affecting screen outcomes.

Gene set enrichment analysis (GSEA) for each screen identified core cellular processes, including translation, RNA splicing, and DNA replication, among others (Figures 2D and S3A–S3C; Table S4). This indicated that the screens were effective at revealing essential gene targets, which is consistent with previous use of this library (Shalem et al., 2014). Interestingly, however, each screen was enriched for genes involved in cerebrum and CNS development, suggesting that each of the isolates retains the function of brain-specific gene networks (Figure 2E). Closer examination of these hits revealed genes with critical roles in regulating asymmetric and symmetric divisions of neural progenitors during cortical development (Figure 2F)(Sun and Hevner, 2014), consistent with GSCs and NSCs sharing underlying neuroprogenitor biology.

Interestingly, among hits specifically enriched in NSCs screens, but not GSCs, were sgRNAs belonging to the Fanconi anemia pathway gene network (Figures 2F and S3D), which is required to suppress apoptosis in mouse neural progenitors (Sun and Hevner, 2014), and also a network of citric acid cycle and respiratory electron transport genes (Figure S3D). The latter is consistent with the notion that GBM cells experience the Warburg effect where metabolism shifts from oxidative phosphorylation to lactate production (Wu et al., 2014).

GSC-Specific CRISPR-Cas9 Screen Hits Fall Outside of Core Genes and Pathways Altered in GBM

We next wondered whether our screen hits would be biased toward inclusion of gene hits found in networks and pathways commonly found altered in GBM and in our patient isolates. For example, the concept of "oncogene addiction" predicts that cancer cells should differentially require oncogene activities to which they are "addicted" (Weinstein and Joe, 2008). To this end, patient-specific GBM networks were created by mapping the results from genomic data from GSC-0131 and GSC-0827 (i.e., RNA-seq, CNV, and exome-seq) onto genes and pathways commonly altered in GBM from TCGA data (e.g., p53, PI3K, Rb-Axis, etc.) (Figure S4). We then incorporated GSC specific lethal screens hits, which also did not score in NSCs (to model therapeutic window).

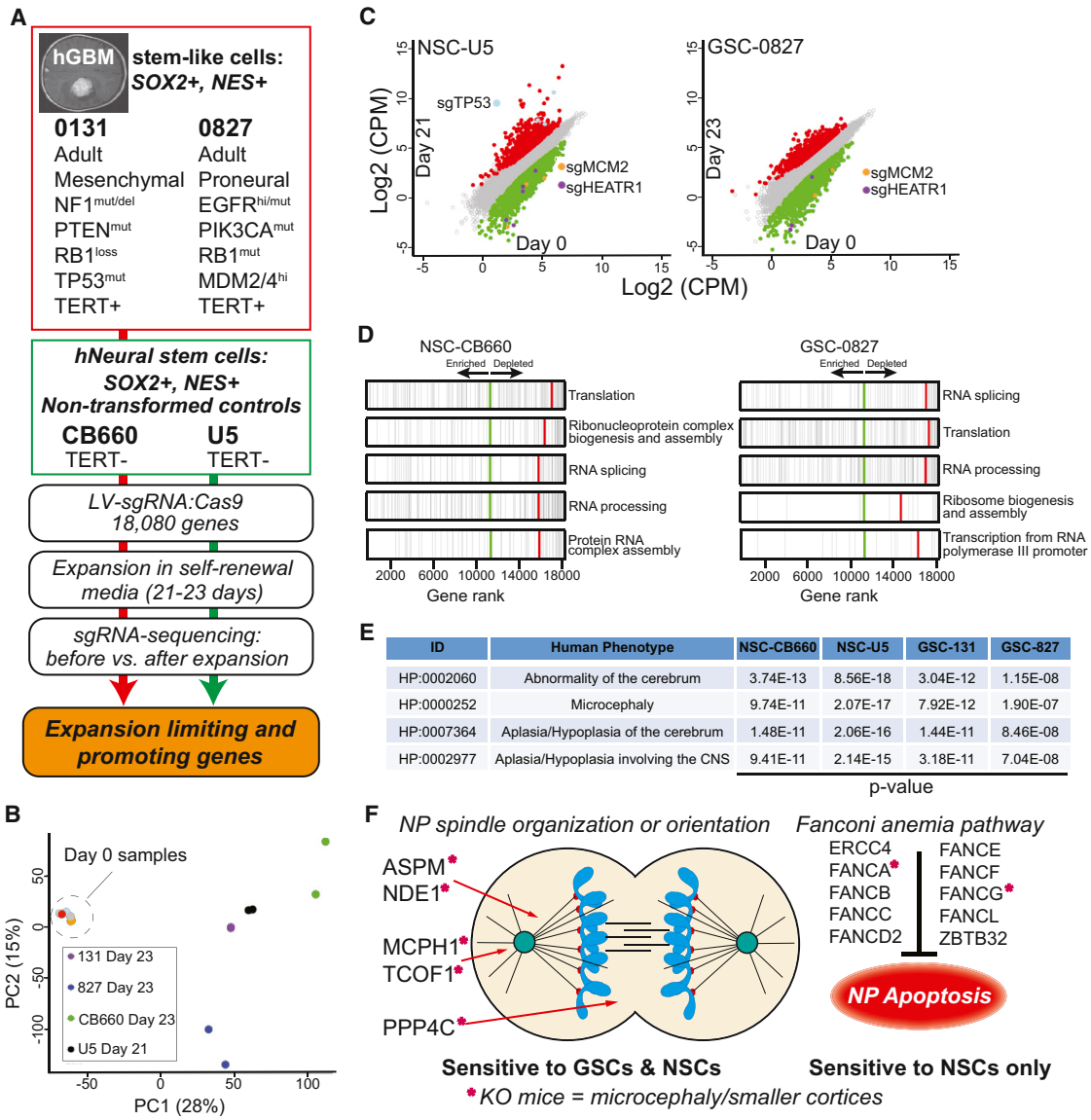

ID	Human Phenotype	NSC-CB660	NSC-U5	GSC-131	GSC-827
HP:0002060	Abnormality of the cerebrum	3.74E-13	8.56E-18	3.04E-12	1.15E-08
HP:0000252	Microcephaly	9.74E-11	2.07E-17	7.92E-12	1.90E-07
HP:0007364	Aplasia/Hypoplasia of the cerebrum	1.48E-11	2.06E-16	1.44E-11	8.46E-08
HP:0002977	Aplasia/Hypoplasia involving the CNS	9.41E-11	2.14E-15	3.18E-11	7.04E-08

Figure 2. Genome-wide CRISPR-Cas9 KO Screens in GSCs and NSCs

(A) Overview of GSC and NSC isolates used and screen procedure.

(B) Principal component analysis of sgRNA-sequencing results of biological screen replicates.

(C) Scatterplots showing log2 normalized library sgRNA read counts comparing day 21 or 23 to day 0 . Each dot represents a specific sgRNAs. Red dots indicate significantly overrepresented sgRNAs (LogFC >1, false discover rate [FDR] <0.05), while green dots indicate significantly underrepresented sgRNAs (LogFC <−1, FDR <0.05) after outgrowth. HEATR1 and MCM2 were top scoring essential gene hits, while TP53 showed strong enrichment in NSC screens.

(D) GSEA for gene ontology biological processes terms was conducted on all sgRNAs from screen results. Top 5 depleted gene sets in NSC-CB660 (FDR-corrected q < 0.0001) and GSC-0827 (FDR-corrected q < 0.011, 0.010, 0.012, 0.057, and 0.070 respectively) are displayed. Green line represents the point where the ratios (end point of screen/day 0) change from positive (left) to negative (right). Red line represents the point where the running sum statistic has its maximum deviation from 0 (enrichment score).

(E) Overlapping human phenotype ontology gene sets enriched among candidate sensitive hits (logFC < −1.0, FDR < 0.05). Each set shown was among top ten gene sets enriched.

(F) Significant screen hits (logFC <−1, FDR <0.05) were overlapped with genes involved in cortical neural progenitor (NP) organization or orientation and the Fanconi anemia pathway. A gene was scored if one or more sgRNA(s) per gene met the criterion.

Surprisingly, only 10 GSC-specific hits out of 946 total (Figure 2A) overlapped core pathways altered in GBM (Figure S4A). For GSC-0131s, only four genes were in the network: *CCNE1*, *MLST8*, *SREBF2*, and *TP53*. None of these genes are altered in the descriptive genomics data from these patient samples, except for *TP53*. GSC-0131s have a homozygous $TP53^{V147D}$ mutation (Table S1), which alters the requirement for *MDM2* and *MDM4* (as judged by loss of sgMDM2/4 in $TP53^{wt}$ isolates,

but not GSC-0131s) and how sgRNAs targeting *TP53* score (GSC-0131s possibly have a reliance on mutant TP53) (Figure S1F).

For GSC-0827s, seven screen hits were in its network (i.e., *AKT1*, *ERBB3*, *GAB1*, *MLST8*, *NFKB1*, *PRKCA*, and *PRKCI*) (Figure S4B). Of these, four have missense mutations of unknown function and two are overexpressed (relative to NSCs). However, because this isolate is a mutator (Figure S1D), many genes in the network are altered. GSC-0827s have an activating mutation in *PI3KCA* and also an *EGFR* amplification and mutation. However, these were not among the screen hits. Thus, counter to the notion of "oncogene addiction," this analysis suggested that core pathways altered in GBM are not good predictors of CRISPR-Cas9-based lethality, as the majority of GBM lethal hits (>95%) occur outside of core GBM altered pathways. One caveat though is that we do not know whether each library sgRNA is effective at targeting each gene in the GBM network; another is that these screens are not perfect with respect to precision and recall (Figure S2C) or retest rate (see below).

Validation of Essential and GSC-Sensitive Genes In Vitro and In Vivo

To initially validate lethal screen hits, we created a retest pool consisting of 7 essential genes and 51 GSC-sensitive genes picked with bias toward genes coding for proteins with enzymatic function (e.g., PKMYT1 kinase), or part of complexes with enzymatic activity (e.g., FBXO42 E3 ubiquitin ligase complex) or transcriptional activity (e.g., transcription factor AP-2 gamma, TFAP2C) from edgeR analysis (three to four sgRNAs per gene) comparing GSCs to NSCs sgRNAs with logFC < -1 (Figure 3A). We first examined performance of individual sgRNAs from the pool in in vitro growth assays in NSC-CB660s, GSC-0131s, and GSC-0827s, testing 47 individual sgRNAs (approximately two sgRNAs per gene) (Figures 3B and S5A; Table S6). Of 47 sgRNAs tested, 27 (57%) scored in a manner consistent with the initial screen, which included *PKMYT1*, candidate GSC-sensitive gene, and *HEATR1*, candidate top scoring essential gene that is involved in rDNA transcription (Prieto and McStay, 2007) (Figures 3B and S5A).

Next, we performed parallel screens with the full retest pool both in vitro in GSCs and NSCs and in vivo in tumors derived from GSC cells. For the in vitro retest screens, two biological replicates of NSC-CB660, GSC-0131, and GSC-0827 cell pools were outgrown for 21 days similar to the primary screen. For the in vivo tumor formation, five independently derived tumors were analyzed from GSC-0131s and GSC-0827s infected with the retest pools (Supplemental Experimental Procedures). Like the main screen, the results were assayed by the changes in sgRNA representation either at day 21 for in vitro studies or after tumor formation for in vivo studies compared to day 0. Heatmaps representing the change in representation for all sgRNAs in the pool are shown in Figure 3C for in vitro and in vivo results, with callouts for genes that scored prominently as cancer-sensitive or essential. Analysis of in vitro versus in vivo results for this analysis suggested good concordance of changes in replication (R^2 = 0.59 for GSC-0131s; R^2 = 0.83 for GSC-0827s) (Figures S5B and S5C). GSC-0131s had 22 screen hits displaying significant loss of representation relative to control and EGFP sgRNAs ($\geq$2 sgRNAs with –logFC, $p < 0.05$), while GSC-0827s had 17 screens hits meeting the same criteria (Figures S5B and S5C). Comparing in vitro GSC and NSC data revealed 18 hits with two or more sgRNAs at logFC ≤ -1.0 for GSC-0131 and seven hits meeting the same criteria for GSC-0827 (Figures S5D and S5E). Both in vitro and in vivo retests yielded *PKMYT1* as the top "convergent" GSC-lethal gene. Other hits consistent with original screen results included: *FBXO42* (0827 specific), *HDAC2* (0827 specific), and *TFAP2C* (0131 specific), among others (Figure 3C).

Comparisons with Short Hairpin RNA Screens Performed in GSCs and NSCs

Since the CRISPR-Cas9 screens produced results consistent with identification of GSC-lethal genes, we also compared the results to previously performed genome-wide short hairpin RNA (shRNA) screens conducted in NSC-CB660, GSC-0131, and GSC-0827 cells in identical outgrowth conditions, which also produced GSC-specific hits (Hubert et al., 2013). Consistent with CRISPR-Cas9 screens preferentially identifying essential genes, there was greater number of total "essential hits" in sgRNA screens predicted to be lethal to all isolates (769 versus 95) (Figure S6). There was an agreement between GSC-sensitive hits from both screens for several networks and pathways, including pre-mRNA splicing, which includes genes previously reported as GSC-sensitive involved in 3′ splice-site recognition (Hubert et al., 2013); control of the G2/M transition, including two key negative regulators of cyclin B/CDK1 activity, *PKMYT1* and *WEE1*; DNA damage checkpoint, including *ATRIP*, *MDC1*, and *CLSPN*; members of COP9 signalosome complex (Lee et al., 2011), among others. Importantly, several nodes among these complexes, including *PKMYT1* and *CAB39*, were validated in the course of our sgRNA retests (Figure 3C). The results suggest that these pathways and complexes cross-validate between the two technology platforms as GBM-sensitive.

PKMYT1 KO Causes Lethality in Multiple GSC Isolates

To further evaluate retesting sgRNA screen hits, we next examined targeting of *PKMYT1*, *FBXO42*, *HDAC2*, *TFAP2C*, and *HEATR1* in ten different GSC isolates along with NSCs using in vitro viability assays and two control sgRNAs (Figure 3E). The results revealed that *PKMYT1* was required for viability in eight of these isolates, while *HDAC2* and *TFAP2C* requirement appeared more specific to GSC-0827s and GSC-0131s, respectively. However, targeting of *FBXO42*, which can promote ubiquitination and degradation of p53 (Sun et al., 2009), showed profound sensitivity in both the GSC-0827 and GSC-G166 isolates (Figure 3E). This likely indicates that patient-specific genetic or epigenetic alterations drive differential requirement for these genes. In contrast, *HEATR1* sgRNAs were lethal to all isolates examined (Figure 3E), demonstrating that the differences in GSC-specific requirement for the other genes are not technical artifacts.

Molecular and Phenotypic Analysis of PKMYT1 Depletion

Since *PKMYT1* emerged as a robust GSC-sensitive hit both in vivo and in vitro among our retests, we wished to further validate it as a candidate therapeutic target for GBM. *PKMYT1* (aka

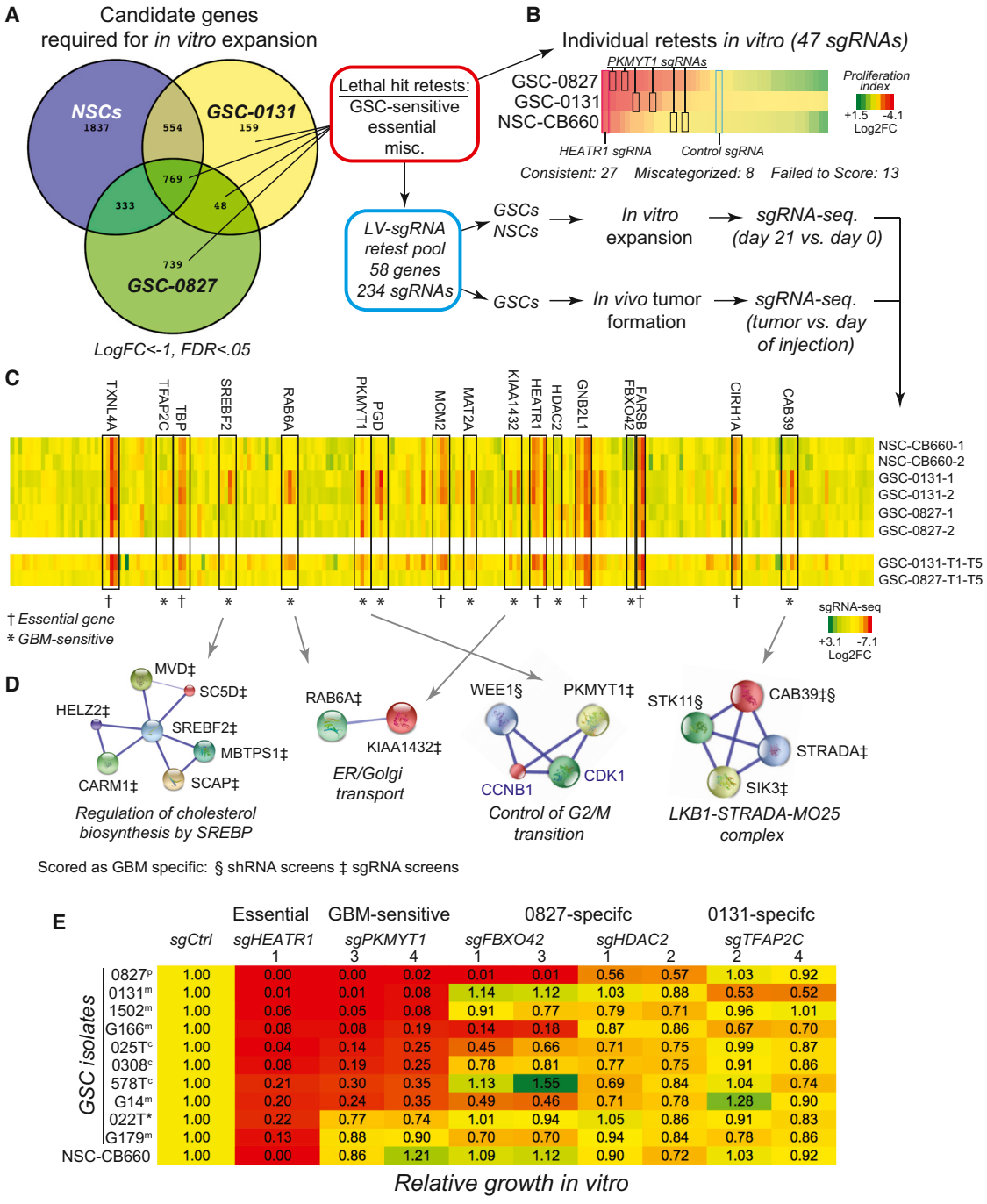

Figure 3. Validation of CRISPR-Cas9 Screen Hits Required for GSC Expansion In Vitro and In Vivo

(A) Venn diagram showing overlap among candidate genes. sgRNAs with logFC <−1.0 (FDR <0.05) were considered candidate sensitive genes. For simplicity, NSC-U5 and NSC-CB660 were combined.

(B) Heatmap of retested candidate sensitive individual sgRNAs (two sgRNAs/gene; 23 genes). Cells were infected with lentivirus containing individual sgRNAs, and cultured (15–22 days) in triplicate. Overall, growth of each sgRNA was calculated and normalized to sgControl. Each sgRNA was categorized as essential, GBM sensitive, or patient-specific according to screen results and then compared. Figure S5 contains sgRNAs scores, Table S5 contains individual sgRNA sequences used in retest, and Table S6 contains source data.

(C) Heatmap of retested in vivo and in vitro pools (58 genes; three to four sgRNAs/gene). For in vivo studies, GSCs were injected into mice (n = 5) following selection (see Supplemental Experimental Procedures). Tumors were cut into two, sequenced, and scored using limma. -T, tumor. Table S6 contains source data.

(D) STRING network (Szklarczyk et al., 2015) representations of GSC-specific hits scoring in pooled retest assays, along with other GSC-specific hits either scoring in CRISPR-Cas9 or shRNA genome-wide screens (see text and also Figure S5 for details of sgRNA and shRNA screen comparisons).

(legend continued on next page)

Myt1) encodes a dual specificity protein kinase homologous to *WEE1* that localizes to the ER-Golgi complex and, at least in vitro, can inhibit cyclin B-CDK1 activity, by phosphorylating CDK1's ATP binding domain at T14 and to a lesser extent Y15 (Booher et al., 1997; Liu et al., 1997). WEE1, by contrast, has been shown to phosphorylate Y15 of both CDK1/2 but is incapable of phosphorylating T14 (Watanabe et al., 1995). Genetic experiments in *Drosophila* suggest that *PKMYT1* and *WEE1* homologs act redundantly during fly development (Jin et al., 2008). However, loss-of-function experiments in mammals, which have been performed mainly in HeLa cells, suggest that human *PKMYT1* and *WEE1* are not functionally equivalent. For example, knockdown of *WEE1* in HeLa cells induces loss of Y15 phosphorylation, premature entry into mitosis before completion of DNA replication (i.e., mitotic catastrophe), and apoptosis (Nakajima et al., 2008),(Coulonval et al., 2011). By contrast, *PKMYT1* knockdown either fails to affect the timing of mitotic entry and exit of HeLa cells or does so modestly, despite dramatically reducing CDK1-T14 phosphorylation, without affecting CDK1-Y15 (Nakajima et al., 2008; Coulonval et al., 2011; Villeneuve et al., 2013). Thus, in mammals it is unclear whether PKMYT1 is required for regulating cyclin B/CDK1 activity during the cell cycle, whereas there is ample evidence that WEE1 activity plays key roles in preventing premature mitosis.

Given our results, we were interested to determine how *PKMYT1* and *WEE1* might have roles in specifically sustaining GSC viability. We began by examining the effects of PKMYT1 and WEE1 inhibition on CDK1/2 T14 and Y15 phosphorylation in our NSC isolates, which permit KO of *PKMYT1* without significant loss of viability (Figure 4A). In NSC-CB660s, we observed that *PKMYT1* KO results in dramatic reduction of PKMYT1 protein and CDK1-T14 phosphorylation with little or no effect on CDK1/2 Y15, consistent with previous studies. However, we find that PKMYT1 does in fact act redundantly with WEE1 to phosphorylate CDK1-Y15 in NSCs. Western blot analysis shows that PKMYT1 activity sustains CDK1-Y15, but not CDK2-Y15, phosphorylation in the presence of a potent and specific WEE1 inhibitor (MK1775) (Figures 4A and 4B).

To investigate these effects phenotypically, we used time-lapse microscopy to measure mitotic transit times (MTTs) (from nuclear envelop break down to cytokinesis). In *Drosophila*, loss of myt1 and wee1 dramatically increases the mitotic index of imaginal wing disc cells (Jin et al., 2008), and a similar phenotype is observed in HeLa cells overexpressing CDK1-T14A-Y15F, which cannot be phosphorylated by PKMYT1 or WEE1 activity (Krek and Nigg, 1991). We reasoned that this is likely due to activation of the spindle assembly checkpoint (SAC), which blocks anaphase until end-on attachment of kinetochores and microtubules has occurred, and chromosomes are properly aligned and stable (Santaguida and Musacchio, 2009); thus, we would expect MTT to be similarly delayed in our cells. First examining NSCs, we find that KO of *PKMYT1* or WEE1 inhibition alone led to modest increases in MTT, where average MTT in control cells is 37 min compared to 47–51 min (Figures 4C and 4D). However, loss of PKMYT1 and WEE1 activity together resulted in synergistic increases in MTTs to over 100 min on average with many cells well over 150 min (Figures 4C and 4D). Importantly, concomitant synergistic increases in cell death during mitosis and cytokinesis failure were also observed (Figure 4E). Visual inspection of double inhibited cells with extended MTTs indicated that they spend most of their time arrested at metaphase, consistent with a SAC-induced arrest (data not shown).

We next repeated the same set of experiments in parallel in NSC-CB660s and GSC-0827s, this time using a small interfering RNA (siRNA) pool to inhibit PKMYT1, which allowed for better control of timing of PKMYT1 inhibition in GSCs. Importantly, the siRNA pool resulted in dramatic loss of PKMYT1 protein expression (Figure 5D). In NSC-CB660s, the siPKMYT1 pool precisely phenocopied the effects of PKMYT1 KO, showing the same increases in MTTs for PKMYT1 alone and together with WEE1 inhibition (Figure 5A). By contrast and strikingly, in GSC-0827s, inhibition of PKMYT1 or WEE1 alone was sufficient to cause dramatic increases in MTTs similar to those observed for double inhibition in NSCs (Figure 5B). As before, extended MTTs were associated with cell death during mitosis and also cytokinesis failure (Figure 5C). However, unlike NSCs, PKMYT1 depletion or WEE1 inhibition alone in GSCs resulted in cell death during mitosis and also cytokinesis failure, and double treatment resulted in the majority of the cells experiencing cell death during mitosis. Consistent with this notion, dose-response curves of WEE1 inhibitor alone also showed that GSCs are particularly sensitive, but not NSC-CB660s (Figure 5F). Furthermore, knockdown of PKMYT1 also compromised growth of GSC-0827s in limiting dilution sphere formation assays, a surrogate assay for self-renewal (Figure 5E). Importantly, these data demonstrate that PKMYT1 and WEE1 are synthetic lethal in NSCs and act redundantly to facilitate mitosis in human NSCs, and that this redundancy is lost in GBM cells, giving rise to differential requirement for PKMYT1.

Oncogenic Activation of *EGFR* and *AKT1* Sensitize NSCs to Loss of PKMYT1 Function

We next wondered what could cause loss of *PKMYT1* and *WEE1* redundancy in GSCs. Previous studies have established that the AKT and MAP kinase pathways can negatively impact PKMYT1 or WEE1 activity during meiosis/oocyte maturation (Okumura et al., 2002; Palmer et al., 1998) and the somatic cell cycle (Katayama et al., 2005; Villeneuve et al., 2013). In human cells, AKT has been shown to directly phosphorylate WEE1 at Ser-642, causing its retention in the cytoplasm and loss of WEE1 activity (Katayama et al., 2005). In addition, MEK1 activity has been implicated in downregulation of PKMYT1 activity as HeLa cells enter mitosis (Villeneuve et al., 2013). Since activation of PI3K and RTK signaling cascades are prominent features of GBM tumors, we next asked whether altering these pathways would be sufficient to trigger *PKMYT1* KO sensitivity in our NSCs.

(E) In vitro viability assays retesting individual sgRNAs in multiple GSC isolates of different TCGA subtypes for genes indicated. Samples were outgrown for 12 days following selection or cultured for 18 days following selection and counted with each split every 5–7 days to determine total cell number and normalized to sgControl. See Table S6 for Student's t tests. TCGA subtypes: p, proneural; m, mesenchymalm; c, classical; or *, unable to classify (see Table S7 and Supplemental Experimental Procedures for details).

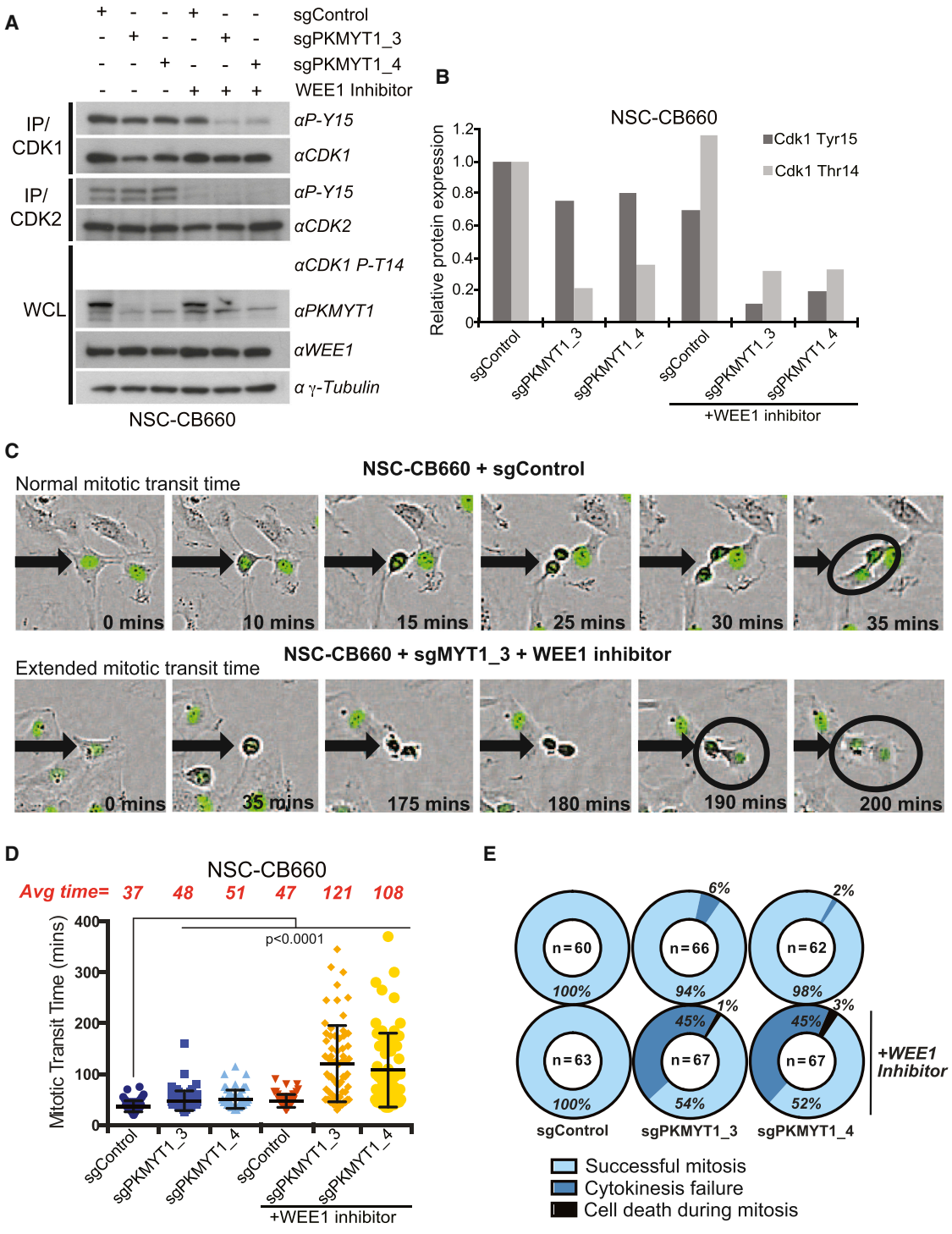

Figure 4. Molecular and Phenotypic Characterization of *PKMYT1* Function in GSCs and NSCs

(A) *PKMYT1* and *WEE1* act redundantly to phosphorylate Cdk1-Y15 in NSC-CB660s. Western blot analysis on whole-cell lysates (WCLs) or following immunoprecipitation (IP) of *CDK1* or *CDK2*. NSC-CB660s were outgrown for 14 days following selection and then treated with 300 nM of MK1775 (WEE1 inhibitor) for 6 hr or mock treated. PKMYT1 antibody recognizes a non-specific protein that appears below *PKMYT1* predicted molecular weight.

(B) Semi-quantification of western blot in (A) using ImageJ. Each band was normalized to their respective sgControl (-MK1775) sample.

(C) Representative images from time-lapse microscopy. NSC-CB660s were transduced with individual sgPKMTY1 and sgControl LV constructs, selected for 4 days, and outgrown for 15 days. Cells were then treated with 300 nM of the WEE1 inhibitor MK1775 or mock treated, followed by time-lapse microscopy for 72 hr. Images were acquired at 50-min intervals. Mitotic transit time was analyzed for individual cells following 6 hr of WEE1 inhibition.

(legend continued on next page)

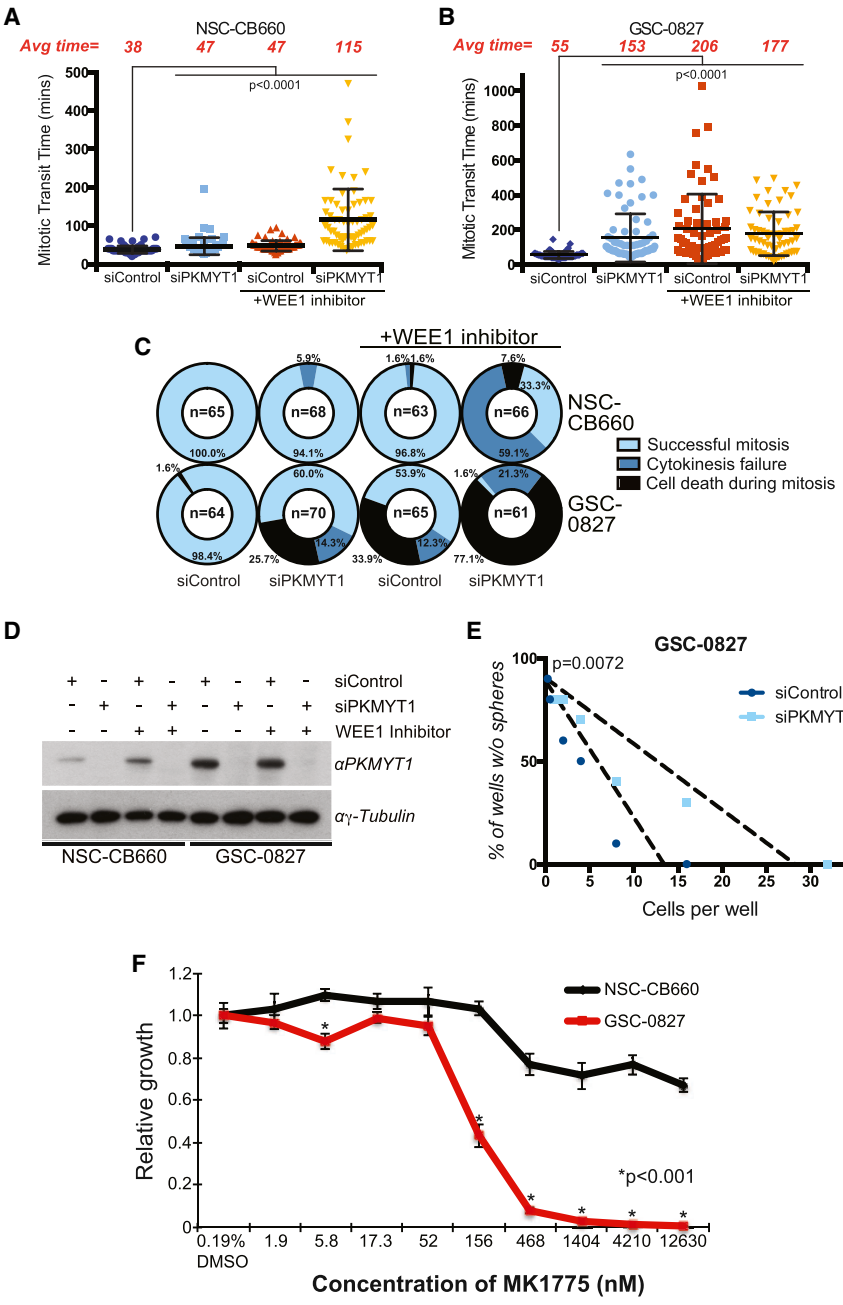

Figure 5. Loss of PKMYT1 and WEE1 Redundancy in GSC-0827 Cells

(A and B) Quantitation of mitotic transit times (MTTs) of individual NSC-CB660s (A) and GSC-0827s from (B) after *PKMYT1* depletion, –/+ WEE1 inhibition (minimum of 6 hr). Cells were transfected, treated with MK1775 (300 nM) or mock treated (48 hr after initial transfection), and subjected to time-lapse microscopy for 48 hr. Mann-Whitney test; n ≥ 60 cells/condition; ±SD.

(C) Outcome of each mitosis from cells counted in (A) and (B).

(D) Protein expression levels of PKMYT1 depletion by RNAi –/+ WEE1 inhibition in NSCs and GSCs. PKMYT1 depletion with siRNAs in NSC-CB660 and GSC-0827 –/+ MK1775 (WEE1 inhibitor). Western blot analysis on whole-cell extracts that were transfected with siControl or siPKMYT1 (see Supplemental Experimental Procedures) for 24 hr. Following 48 hr from the initial transfection, cells were treated with 300 nM of MK1775 (WEE1 inhibitor) for 6 hr or mock treated and harvested for protein extraction.

(E) Limiting dilution sphere formation assays for GSC-0827s that were treated to knockdown PKMYT1. Cells were transfected with siControl or siPKMYT1 for 24 hr. Cells were then harvested and plated into 96-well plates at various seeding densities (0.125–256 cells per well, ten wells per condition). Linear regression analysis was performed to generate each line per sample, and then each line was compared (p value).

(F) WEE1 inhibitor dose-response curves for NSC-CB660s and GSC-0827s. A differential response is observed between NSC-CB660s and GSC-0827s treated with the WEE1 inhibitor MK1775. Cells were plated into 96-well plates and treated with various doses of the WEE1 inhibitor dissolved in 0.18% DMSO 24 hr later. Following 72 hr post-treatment, viability was assessed using CellTiter-glo (Promega). Samples were normalized to the DMSO only control sample, and the viability of GSC-0827s was compared to NSC-CB660s at each dose (Student's t test [unpaired, unequal variance]; five to six replicates per dose for each line).

To this end, we used constitutively active alleles of *EGFR* (EGFRvIII)* (Bachoo et al., 2002) and *AKT1** (myristoylation tagged) (Boehm et al., 2007) in combination with *TERT*, dominant-negative $TP53^{DD}$, and $CCND1^{+}CDK4^{R24C}$ (p16 resistant) (Kendall et al., 2005) in NSC-CB660s. Note that manipulating the p53 and Rb axis is required to bypass *EGFR** induced senescence or apoptosis in our NSCs. Figures 6A and 6B shows the consequences of various combinations of these human oncogenes on CDK1-T14 and CDK1/2-Y15 phosphorylation levels. Interestingly, adding *EGFR** and then *AKT1** to these cells dramatically suppressed T14 and Y15 phosphorylation to ~2-fold below the baseline found in NSCs and >3-fold from levels found in *TP53/RB*-axis altered cells (which were higher than baseline). *AKT1** alone, however, had no effect. Instead,

(D) Quantitation of mitotic transit times (MTTs) of individual NSC-CB660s from (C) after *PKMYT1* KO, –/+ WEE1 inhibition (minimum of 6 hr). NSC-CB660s were outgrown for 15 days following selection, treated with MK1775 (300 nM) or mock treated, and subjected to time-lapse microscopy for 72 hr. Mann-Whitney test; n ≥ 60 cells/condition; ±SD.

(E) Quantification of phenotypic outcome of mitosis from (C) and (D). See Supplemental Experimental Procedures for details. A cell was considered to enter mitosis when nuclear envelope breakdown was visible.

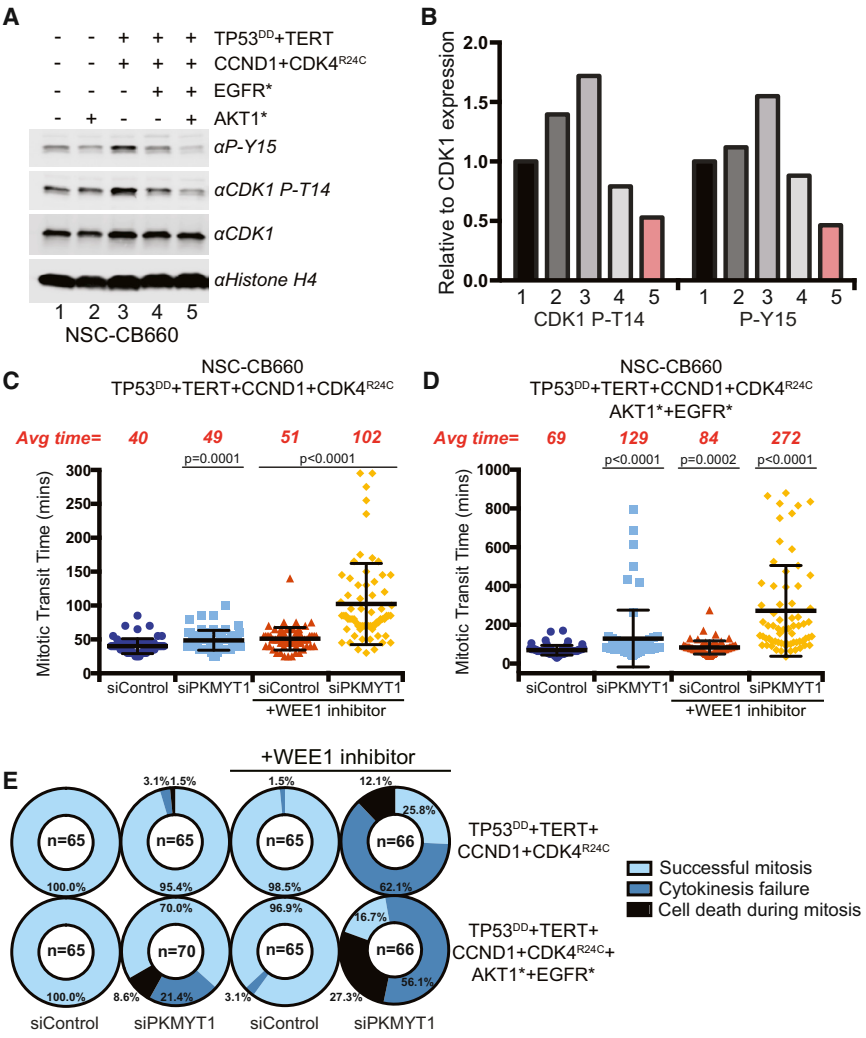

Figure 6. Expression of Constitutively Active Alleles of *EGFR* and *AKT* Sensitize NSCs to *PKMYT1* Depletion

(A and B) *EGFR** and *AKT** cause depletion of steady-state levels of CDK1/2-Y15 and CDK1-T14 phosphorylation in NSC-CB660s. (A) Western blot analysis of total CDK1/2-Y15-P and CDK1-T14-P using whole-cell lysates (WCL). Histone H4 was used as a loading control. Lane number corresponds to its respective number in (B). Note that p53 and RB-axis pathway perturbations are required to bypass EGFR*-induced senescence and apoptosis in NSCs. Thus, EGFR* experiments could not be carried out alone. (B) Semi-quantitative analysis of western blot from (A). Samples were first normalized to their respective loading control followed by their respective *CDK1* expression.

(C and D) Mitotic transit time of individual genetically altered NSCs after PKMYT1 depletion, –/+ WEE1 inhibition (minimum of 6 hr). Cells were transfected, treated with MK1775 (300 nM) or mock treated (48 hr after initial transfection), and subjected to time-lapse microscopy for 48 hr. Mann-Whitney test; n ≥ 65 cells/condition; ±SD.

(E) Outcome of each mitosis from cells counted in (C) and (D).

*AKT1** potentiated the effect of *EGFR**. These results demonstrate that activation of the EGFR and AKT pathways is sufficient to suppress the steady-state levels of CDK1-T14 and CDK1/2-Y15 phosphorylation in NSCs.

To determine whether *EGFR** and *AKT1** affected the requirement for *PKMYT1*, we again performed MTT assays. We found that NSC-CB660s with *TERT*TP53DD+CCND1*CDK4R24C* behaved exactly like unmanipulated NSCs (Figure 6C). Importantly, however, the addition of *EGFR** and *AKT1** to these cells in the presence of siPKMYT1 produces similar effects on MTTs that were observed for GSCs (Figure 6D), where siPKMYT1 almost doubled MTTs. This pattern also extends to increases in frequency of unsuccessful mitoses (Figure 6E), with dramatic increases in cell death during mitosis and cytokinesis failure. It is also interesting to note that EGFR* and AKT* expression in control experiments increased NSC MTTs from 40 to 69 min, as GSC-0827s show a similar trend. Taken together, these results suggest that overactive EGFR and PI3K signaling is sufficient to cause loss of redundancy between *PKMYT1* and *WEE1* and differential sensitivity to loss of *PKMYT1*, suggesting a general mechanism for *PKMYT1* requirement in GSCs.

Examining CRISPR-Cas9-Triggered Insertion-Deletion Mutation Formation

Last, we confirmed sgRNA:Cas9 on-target nuclease activity by deep sequencing target sites for multiple sgRNAs scoring in our screens. While we observed high frequencies of on-target indel formation (Figures 7 and S7), consistent with other recent studies (Bae et al., 2014; Shalem et al., 2014), we found unexpected biases in mutation spectra. In many cases, single nucleotide insertions were dramatically overrepresented (Figures 7B and 7C), biasing indels toward reading frameshifts. In fact, only one of the seven sgRNA-target site combinations tested showed nearly unbiased reading frameshifts after indel formation, which would be expected to occur one-third of the time (Figure 7D). Without this bias, small indels would have little affect on gene function nearly a third of the time. Thereby, frameshift bias helps explain the highly penetrant phenotypic effects produced by this technology in human cells.

DISCUSSION

Here, we report the successful application of gene editing technology to identify and characterize genes promoting symmetric in vitro expansion in human GSCs and NSCs. Our results contribute to a growing body of work demonstrating the power

of CRISPR-Cas9 based approaches in human cells to identify context-specific and generally lethal genes (Blomen et al., 2015; Shi et al., 2015; Wang et al., 2015), in our case, using the technology directly in patient-derived tumor isolates. Although sgRNA-triggered KOs may not precisely replicate scenarios with small molecule inhibitors, they do provide clues as to which pathways and genes are likely to trigger a therapeutic response.

Our results speak to the notion of what counts as a good mono-therapeutic target for GBM. From our screen results, we expected to confirm the concept of ''oncogene addiction'' for GBM, or that cancer cells become ''addicted'' to certain oncogene activities during their evolution, such that these activities represent ''rationale'' therapeutic targets (Weinstein and Joe, 2008). However, we found very little overlap between GSC-specific screen hits and genes and pathways altered in GBM in general or in the patient GSC isolates in which the screens were performed. Perhaps most importantly, we could not use descriptive data sets from our patient samples to predict screen outcome (and, thus, candidate therapeutic targets), which is what current precision oncology paradigms attempt to do. While this does not disprove the oncogene addiction hypothesis for GBM, it does suggest that targeting sensitivities caused by oncogenic activity, rather than the oncogenic activities themselves, may provide better therapeutic opportunities. This appears to be a recurring theme in our GBM work, as each of our previous GSC-specific vulnerabilities found by shRNA screening (Hubert et al., 2013; Ding et al., 2013; Toledo et al., 2014) are likely caused by oncogene-induced changes in feedback regulation of the underlying pathways.

Our screen results revealed at least two classes of GSC-specific screen hits that arise from ''individual-specific'' dependencies found uniquely in patient samples and also ''convergent'' dependencies shared between the patient samples. Individual dependences likely arise from the specific epigenetic and genetic alterations arising during patient tumor evolution. While we were able to successfully retest several screen hits specific to GSC-0131 and GSC-0827 (e.g., *FBXO42*, *HDAC2*, *TFAP2C*), we were unable to find evidence that these hits correlated with a specific CNV, mutation, or transcriptional signature from patient samples. More systematic testing of these hits (e.g., larger sample size of GSCs and comprehensive retesting of all hits) will be required to determine whether they are truly unique to these isolates.

Convergent screen hits, which score in multiple GSCs regardless of particular oncogenic alterations, are more interesting from a therapeutic perspective. We predict these to arise from general oncogenic pathway activity rather than specific alterations in pathways. Thereby, it is conceivable that convergent screen hits may represent therapeutic targets that when inhibited are capable of producing durable responses in heterogeneous GBM tumors. Importantly, our follow-up experiments for one such convergent hit, *PKMYT1*, suggests this would indeed be the case. *PKMYT1* arose from screens in patient isolates representing different developmental subtypes (e.g., proneural versus mesenchymal) and also distinct genetic alterations (e.g., *EGFR** versus *NF1* loss and *PTEN* loss versus *PI3KCA* activation). Further, *PKMYT1* dependency could be reproduced in NSCs through ectopic activation of receptor tyrosine kinase and PI3K pathways. This suggests that *PKMYT1* inhibition is synthetic lethal with increased activity of these pathways, but not the particular lesions per se found in the patient isolates. Arguably, this makes *PKMYT1* a very intriguing GBM candidate therapeutic target.

From a biological standpoint, our results help re-discover *PKMYT1* function in human cells. PKMYT1 has largely been overlooked as a key player in cell-cycle regulation in mammals, despite convincing evidence in model metazoan systems that it plays key roles in regulating cyclin B/CDK1 activity during meiosis/oocyte maturation (Okumura et al., 2002; Palmer et al., 1998) and entry into mitosis (Jin et al., 2008; Mueller et al., 1995). We find that, in human NSCs, *PKMYT1* acts redundantly with *WEE1* to both maintain CDK1-Y-15 phosphorylation and to promote timely completion of mitosis. Previous work in HeLa cells has demonstrated sole reliance on WEE1 for CDK1-Y-15-P and preventing premature entry into mitosis and mitotic catastrophe (Coulonval et al., 2011; Nakajima et al., 2008). Our data, however, demonstrate that *PKMYT1* activity can compensate for both Y-15-P and preventing extended MTTs in WEE1 inhibited non-transformed NSCs (Figure 4). This is consistent with the observation that *Drosophila* wee1 and myt1 have redundant and overlapping roles during fly development (Jin et al., 2008). We predict that the same redundancy will be observed in other *non-transformed* vertebrate cell types.

We attribute the observed GSC-specific lethality of *PKMYT1* KO to loss of redundancy of PKMYT1 and WEE1. In GSCs, *PKMYT1* loss alone leads to dramatic increases in MTTs, as well as cell death during mitosis and cytokinesis failures (Figure 5).

We show that activation of EGFR and AKT1 pathways suppress CDK1/2-Y15 and CDK1-T14 phosphorylation in NSCs (Figure 6). This strongly suggests that activation of these pathways together results in net loss of inhibition of CDK1/2 during the G2/M transition. It is conceivable that these effects are mediated by direct negative regulation of PKMYT1 or WEE1 activity. However, other mechanisms are possible. This includes directly or indirect regulation of the activity of CDC25 phosphatase, which is responsible for removing CDK-T14 and Y15 phosphorylation and which has been shown to be a target of EGFR signaling in a *Drosophila* model of glioma (Read et al., 2009). Future experiments will be required to address whether EGFR and AKT signaling acts through direct or indirect regulation of PKMYT1 and/or WEE1 activity in GBM cells.

While *PKMYT1* function has not previously been studied in GBM or other cancers, there has been great interest in WEE1 as a potential therapeutic target as a cytotoxic chemotherapy and radiation sensitizer, since it is required for radiation-induced arrest and repair (De Witt Hamer et al., 2011; Mir et al., 2010). For GBM, GSCs appear more resistant to radiation through increased repair proficiency (Bao et al., 2006; Liu et al., 2006). Thus, WEE1 inhibition may enhance radiation treatment. Though the WEE1 inhibitor, MK1775, and temozolomide preclinical combinational studies in mouse flank GBM models were highly effective, the combinational treatment in mouse brain orthotopic xenograft models were ineffective due to the limited heterogeneous distribution of MK1775 across the blood-brain barrier

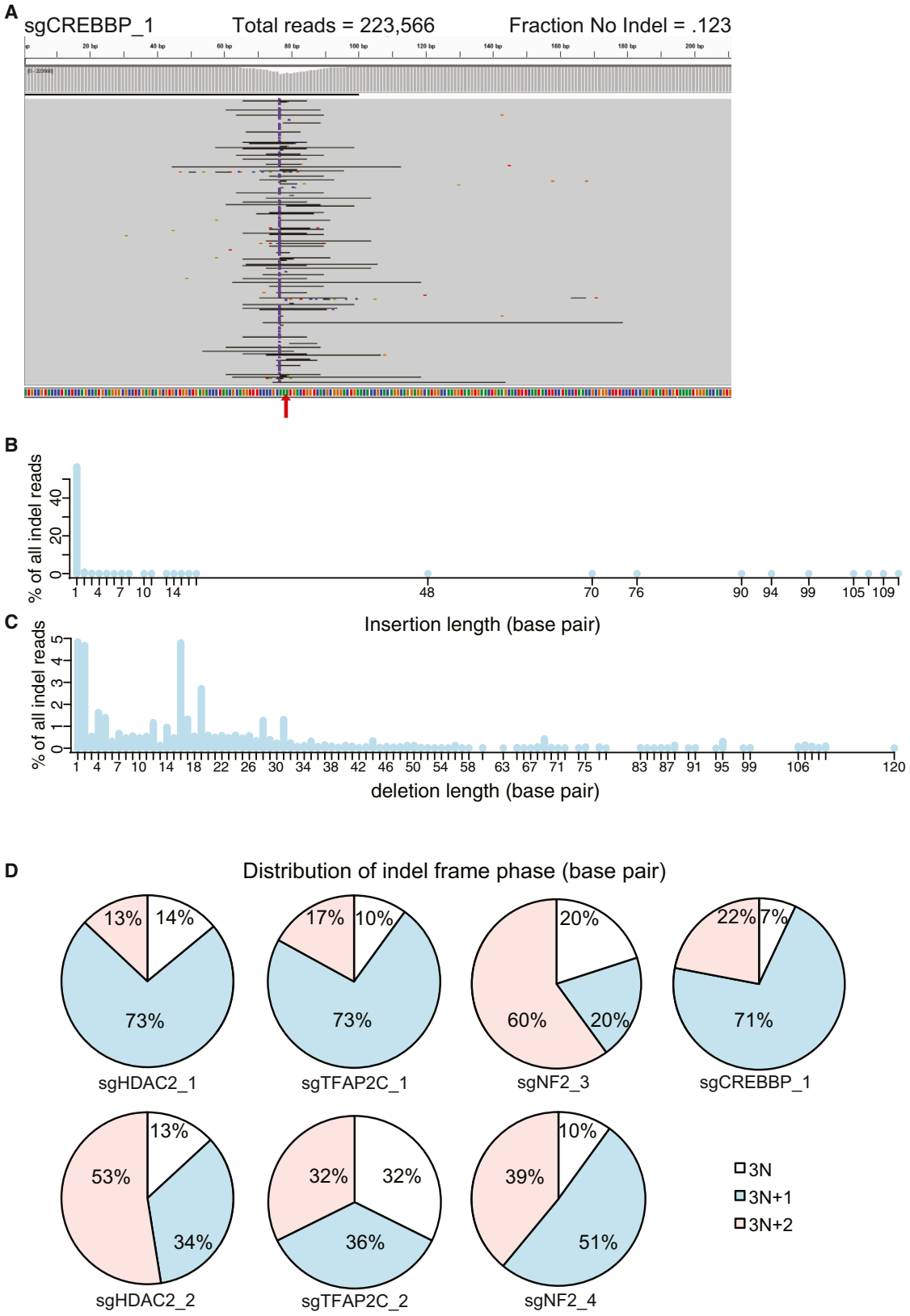

(legend on next page)

(Pokorny et al., 2015). Because the current WEE1 inhibitor in clinical trials is not effective in penetrating the blood-brain barrier, future studies are warranted in order to identify PKMYT1-specific inhibitors, as our results suggest that inhibiting PKMYT1's kinase activity alone may be a GBM-therapeutic target. However, it is currently unclear whether PKMYT1 inhibition would synergize with cytotoxic therapies that engage WEE1 or whether this could suppress requirement for PKMYT1. Future studies will have to address this and also create pipelines for the identification of PKMYT1-specific inhibitors, which, to our knowledge, have not been successfully developed (Rohe et al., 2014a, 2014b).

EXPERIMENTAL PROCEDURES

All in vivo experiments were conducted in accordance with the NIH Guide for the Care and Use of Experimental Animals, and with approval from the Fred Hutchinson Cancer Research Center Institutional Animal Care and Use Committee (IR#1457).

Cell Culture

GSC and NSC lines were grown in N2B27 neural basal media (STEMCELL Technologies) supplemented with EGF and FGF-2 (20 ng/ml) (PeproTech) on laminin (Sigma) -coated polystyrene plates and passaged as previously described (Pollard et al., 2009).

CRISPR-Cas9 Screening

A human genome-wide CRISPR-Cas9 library (Shalem et al., 2014) was used in lentiviral pooled format to transduce GSCs and NSCs. For each screen replicate, cells were transduced at ~500-fold representation of the library (at 30% infection efficiency). 2 days after transduction, puromycin was added (1–4 μg/ml) for 3 days. A portion of cells were harvested as day 0 time point. The rest of the cells were then passaged to maintain 500-fold representation and cultured for an additional 21–23 days (eight to ten cell doublings). Genomic DNA was extracted, and a two-step PCR procedure was employed to amplify sgRNA sequences and then to incorporate deep sequencing primer sites onto sgRNA amplicons. Purified PCR products were sequenced using HiSeq 2500 (Illumina). Raw and mapped data files are available at the Gene Expression Omnibus databasae (GEO: GSE70038).

Additional experimental procedures are available in Supplemental Information.

SUPPLEMENTAL INFORMATION

Supplemental Information includes Supplemental Experimental Procedures, seven figures, and seven tables and can be found with this article online at http://dx.doi.org/10.1016/j.celrep.2015.11.021.

AUTHOR CONTRIBUTIONS

C.M.T., Y.D., P.H., R.J.D., E.J.G., B.E.C., J.M.O., and P.J.P. conceived of and designed the experiments. C.M.T., Y.D., P.H., R.J.D., and E.J.G. performed the experiments. Q.L., X.-N.L., D.-H.N., J.L., and S.M.P. provided cell isolates. R.B., E.L., T.H., H.B., J.D., Q.Z., J.H., B.J.A., C.L.P., N.S.B., J.M., J.Z., and J.J.D. analyzed the data. C.M.T., Y.D., P.H., and P.J.P. wrote the paper.

ACKNOWLEDGMENTS

We thank Prashant Mali, Eric Holland, Pierre Roger, Cassie Sather, and members of J.M.O.'s and P.J.P.'s labs for helpful discussions and Pam Lindberg for administrative assistance. We thank Feng Zhang, Prashant Mali, David Sabatini, Valeri Vasioukhin, and Denise Galloway for providing reagents. We thank Cory McCartan, Chris Yang, and Christina Toledo for assistance with experiments. This work was supported by the following grants: National Science Foundation Graduate Research Fellowship Program (DGE-0-718124 and DGE-1256082) (C.M.T.), Interdisciplinary Training in Cancer Research (T32CA080416) (P.H.), NCI/NIH (R01CA084069-11) (B.E.C.), NCI/NIH (R01CA155360; R01CA114567) (J.M.O.), NCI/NIH (R01CA190957; R21CA170722; P30CA15704) (P.J.P.), DoD Translational New Investigator Award CA100735 (P.J.P.), the Pew Biomedical Scholars Program (P.J.P.), and a Phi Beta Psi Sorority Cancer Research Grant (P.J.P.).

Received: September 1, 2015
Revised: October 12, 2015
Accepted: November 3, 2015
Published: December 3, 2015

REFERENCES

American Cancer Society. (2010). Cancer Facts and Figures.

Bachoo, R.M., Maher, E.A., Ligon, K.L., Sharpless, N.E., Chan, S.S., You, M.J., Tang, Y., DeFrances, J., Stover, E., Weissleder, R., et al. (2002). Epidermal growth factor receptor and Ink4a/Arf: convergent mechanisms governing terminal differentiation and transformation along the neural stem cell to astrocyte axis. Cancer Cell *1*, 269–277.

Bae, S., Kweon, J., Kim, H.S., and Kim, J.S. (2014). Microhomology-based choice of Cas9 nuclease target sites. Nat. Methods *11*, 705–706.

Bao, S., Wu, Q., McLendon, R.E., Hao, Y., Shi, Q., Hjelmeland, A.B., Dewhirst, M.W., Bigner, D.D., and Rich, J.N. (2006). Glioma stem cells promote radioresistance by preferential activation of the DNA damage response. Nature *444*, 756–760.

Blomen, V.A., Májek, P., Jae, L.T., Bigenzahn, J.W., Nieuwenhuis, J., Staring, J., Sacco, R., van Diemen, F.R., Olk, N., Stukalov, A., et al. (2015). Gene essentiality and synthetic lethality in haploid human cells. Science, Published online October 15, 2015.

Boehm, J.S., Zhao, J.J., Yao, J., Kim, S.Y., Firestein, R., Dunn, I.F., Sjostrom, S.K., Garraway, L.A., Weremowicz, S., Richardson, A.L., et al. (2007). Integrative genomic approaches identify IKBKE as a breast cancer oncogene. Cell *129*, 1065–1079.

Booher, R.N., Holman, P.S., and Fattaey, A. (1997). Human Myt1 is a cell cycle-regulated kinase that inhibits Cdc2 but not Cdk2 activity. J. Biol. Chem. *272*, 22300–22306.

Brennan, C.W., Verhaak, R.G., McKenna, A., Campos, B., Noushmehr, H., Salama, S.R., Zheng, S., Chakravarty, D., Sanborn, J.Z., Berman, S.H., et al.;

Figure 7. Analysis of Mutation Induction by sgRNAs for Various Validating Screen Hits in NSC-CB660 Cells

Cells were transduced with individual sgRNAs to CREBBP, NF2, TFAP2C, or HDAC2 at MOI <1, selected, and outgrown for 12 days (sgCREBBP) or 21 days (remaining sgRNAs). The ~250 bp around the target locus was then PCR amplified and deep sequenced. Note that CREBBP and NF2 were among top enriched sgRNAs in NSC screens (Table S2).

(A) Integrative Genomics Viewer (IGV) image of 220 representative deep sequencing reads for sgCREBBP_1. Red arrow denotes predicted Cas9 cutting site. Four-colored line above the red arrow shows the reference sequence. Black or purple bars in gray sequencing reads indicate deletions or insertions, respectively. Other colors within gray sequencing reads indicate SNPs, possibly due to PCR or sequencing error.

(B) Frequency and distribution of insertion length for sgCREBBP_1.

(C) Frequency and distribution of deletion length for sgCREBBP_1.

(D) Frame phase of all indels for each of the seven sgRNA samples, calculated as the length of indels modulus 3. Note that 3N equals in-frame.

TCGA Research Network (2013). The somatic genomic landscape of glioblastoma. Cell *155*, 462–477.

Chudnovsky, Y., Kim, D., Zheng, S., Whyte, W.A., Bansal, M., Bray, M.A., Gopal, S., Theisen, M.A., Bilodeau, S., Thiru, P., et al. (2014). ZFHX4 interacts with the NuRD core member CHD4 and regulates the glioblastoma tumor-initiating cell state. Cell Rep. *6*, 313–324.

Coulonval, K., Kooken, H., and Roger, P.P. (2011). Coupling of T161 and T14 phosphorylations protects cyclin B-CDK1 from premature activation. Mol. Biol. Cell *22*, 3971–3985.

Dai, Z., Sheridan, J.M., Gearing, L.J., Moore, D.L., Su, S., Wormald, S., Wilcox, S., O'Connor, L., Dickins, R.A., Blewitt, M.E., and Ritchie, M.E. (2014). edgeR: a versatile tool for the analysis of shRNA-seq and CRISPR-Cas9 genetic screens. F1000Res. *3*, 95.

De Witt Hamer, P.C., Mir, S.E., Noske, D., Van Noorden, C.J., and Würdinger, T. (2011). WEE1 kinase targeting combined with DNA-damaging cancer therapy catalyzes mitotic catastrophe. Clin. Cancer Res. *17*, 4200–4207.

Ding, Y., Hubert, C.G., Herman, J., Corrin, P., Toledo, C.M., Skutt-Kakaria, K., Vazquez, J., Basom, R., Zhang, B., Risler, J.K., et al. (2013). Cancer-Specific requirement for BUB1B/BUBR1 in human brain tumor isolates and genetically transformed cells. Cancer Discov. *3*, 198–211.

Gargiulo, G., Cesaroni, M., Serresi, M., de Vries, N., Hulsman, D., Bruggeman, S.W., Lancini, C., and van Lohuizen, M. (2013). In vivo RNAi screen for BMI1 targets identifies TGF-β/BMP-ER stress pathways as key regulators of neural- and malignant glioma-stem cell homeostasis. Cancer Cell *23*, 660–676.

Goidts, V., Bageritz, J., Puccio, L., Nakata, S., Zapatka, M., Barbus, S., Toedt, G., Campos, B., Korshunov, A., Momma, S., et al. (2012). RNAi screening in glioma stem-like cells identifies PFKFB4 as a key molecule important for cancer cell survival. Oncogene *31*, 3235–3243.

Hart, T., Brown, K.R., Sircoulomb, F., Rottapel, R., and Moffat, J. (2014). Measuring error rates in genomic perturbation screens: gold standards for human functional genomics. Mol. Syst. Biol. *10*, 733.

Hubert, C.G., Bradley, R.K., Ding, Y., Toledo, C.M., Herman, J., Skutt-Kakaria, K., Girard, E.J., Davison, J., Berndt, J., Corrin, P., et al. (2013). Genome-wide RNAi screens in human brain tumor isolates reveal a novel viability requirement for PHF5A. Genes Dev. *27*, 1032–1045.

Jin, Z., Homola, E., Tiong, S., and Campbell, S.D. (2008). Drosophila myt1 is the major cdk1 inhibitory kinase for wing imaginal disc development. Genetics *180*, 2123–2133.

Katayama, K., Fujita, N., and Tsuruo, T. (2005). Akt/protein kinase B-dependent phosphorylation and inactivation of WEE1Hu promote cell cycle progression at G2/M transition. Mol. Cell. Biol. *25*, 5725–5737.

Kazanis, I., Lathia, J.D., Vadakkan, T.J., Raborn, E., Wan, R., Mughal, M.R., Eckley, D.M., Sasaki, T., Patton, B., Mattson, M.P., et al. (2010). Quiescence and activation of stem and precursor cell populations in the subependymal zone of the mammalian brain are associated with distinct cellular and extracellular matrix signals. J. Neurosci. *30*, 9771–9781.

Kendall, S.D., Linardic, C.M., Adam, S.J., and Counter, C.M. (2005). A network of genetic events sufficient to convert normal human cells to a tumorigenic state. Cancer Res. *65*, 9824–9828.

Kitambi, S.S., Toledo, E.M., Usoskin, D., Wee, S., Harisankar, A., Svensson, R., Sigmundsson, K., Kalderén, C., Niklasson, M., Kundu, S., et al. (2014). Vulnerability of glioblastoma cells to catastrophic vacuolization and death induced by a small molecule. Cell *157*, 313–328.

Krek, W., and Nigg, E.A. (1991). Mutations of p34cdc2 phosphorylation sites induce premature mitotic events in HeLa cells: evidence for a double block to p34cdc2 kinase activation in vertebrates. EMBO J. *10*, 3331–3341.

Lathia, J.D., Li, M., Hall, P.E., Gallagher, J., Hale, J.S., Wu, Q., Venere, M., Levy, E., Rani, M.R., Huang, P., et al. (2012). Laminin alpha 2 enables glioblastoma stem cell growth. Ann. Neurol. *72*, 766–778.

Lee, J., Kotliarova, S., Kotliarov, Y., Li, A., Su, Q., Donin, N.M., Pastorino, S., Purow, B.W., Christopher, N., Zhang, W., et al. (2006). Tumor stem cells derived from glioblastomas cultured in bFGF and EGF more closely mirror the phenotype and genotype of primary tumors than do serum-cultured cell lines. Cancer Cell *9*, 391–403.

Lee, M.H., Zhao, R., Phan, L., and Yeung, S.C. (2011). Roles of COP9 signalosome in cancer. Cell Cycle *10*, 3057–3066.

Liu, F., Stanton, J.J., Wu, Z., and Piwnica-Worms, H. (1997). The human Myt1 kinase preferentially phosphorylates Cdc2 on threonine 14 and localizes to the endoplasmic reticulum and Golgi complex. Mol. Cell. Biol. *17*, 571–583.

Liu, G., Yuan, X., Zeng, Z., Tunici, P., Ng, H., Abdulkadir, I.R., Lu, L., Irvin, D., Black, K.L., and Yu, J.S. (2006). Analysis of gene expression and chemoresistance of CD133+ cancer stem cells in glioblastoma. Mol. Cancer *5*, 67.

Mali, P., Esvelt, K.M., and Church, G.M. (2013). Cas9 as a versatile tool for engineering biology. Nat. Methods *10*, 957–963.

Mir, S.E., De Witt Hamer, P.C., Krawczyk, P.M., Balaj, L., Claes, A., Niers, J.M., Van Tilborg, A.A., Zwinderman, A.H., Geerts, D., Kaspers, G.J., et al. (2010). In silico analysis of kinase expression identifies WEE1 as a gatekeeper against mitotic catastrophe in glioblastoma. Cancer Cell *18*, 244–257.

Mueller, P.R., Coleman, T.R., Kumagai, A., and Dunphy, W.G. (1995). Myt1: a membrane-associated inhibitory kinase that phosphorylates Cdc2 on both threonine-14 and tyrosine-15. Science *270*, 86–90.

Nakajima, H., Yonemura, S., Murata, M., Nakamura, N., Piwnica-Worms, H., and Nishida, E. (2008). Myt1 protein kinase is essential for Golgi and ER assembly during mitotic exit. J. Cell Biol. *181*, 89–103.

O'Donnell, M., Langston, L., and Stillman, B. (2013). Principles and concepts of DNA replication in bacteria, archaea, and eukarya. Cold Spring Harb. Perspect. Biol. *5*, Published online July 1, 2013.

Okumura, E., Fukuhara, T., Yoshida, H., Hanada Si, S., Kozutsumi, R., Mori, M., Tachibana, K., and Kishimoto, T. (2002). Akt inhibits Myt1 in the signalling pathway that leads to meiotic G2/M-phase transition. Nat. Cell Biol. *4*, 111–116.

Palmer, A., Gavin, A.C., and Nebreda, A.R. (1998). A link between MAP kinase and p34(cdc2)/cyclin B during oocyte maturation: p90(rsk) phosphorylates and inactivates the p34(cdc2) inhibitory kinase Myt1. EMBO J. *17*, 5037–5047.

Pokorny, J.L., Calligaris, D., Gupta, S.K., Iyekegbe, D.O., Jr., Mueller, D., Bakken, K.K., Carlson, B.L., Schroeder, M.A., Evans, D.L., Lou, Z., et al. (2015). The Efficacy of the Wee1 Inhibitor MK-1775 Combined with Temozolomide Is Limited by Heterogeneous Distribution across the Blood-Brain Barrier in Glioblastoma. Clin. Cancer Res. *21*, 1916–1924.

Pollard, S.M., Yoshikawa, K., Clarke, I.D., Danovi, D., Stricker, S., Russell, R., Bayani, J., Head, R., Lee, M., Bernstein, M., et al. (2009). Glioma stem cell lines expanded in adherent culture have tumor-specific phenotypes and are suitable for chemical and genetic screens. Cell Stem Cell *4*, 568–580.

Prieto, J.L., and McStay, B. (2007). Recruitment of factors linking transcription and processing of pre-rRNA to NOR chromatin is UBF-dependent and occurs independent of transcription in human cells. Genes Dev. *21*, 2041–2054.

Read, R.D., Cavenee, W.K., Furnari, F.B., and Thomas, J.B. (2009). A Drosophila model for EGFR-Ras and PI3K-dependent human glioma. PLoS Genet. *5*, e1000374.

Robinson, M.D., McCarthy, D.J., and Smyth, G.K. (2010). edgeR: a Bioconductor package for differential expression analysis of digital gene expression data. Bioinformatics *26*, 139–140.

Rohe, A., Gollner, C., Erdmann, F., Sippl, W., and Schmidt, M. (2014a). The glycoglycerolipid 1,2-dipalmitoyl-3-(N-palmitoyl-6′-amino-6′-deoxy-alpha-d-glucosyl)-sn-glycerol is no inhibitor of the human Myt1 kinase. J. Enzyme Inhib. Med. Chem. *30*, 514–517.

Rohe, A., Henze, C., Erdmann, F., Sippl, W., and Schmidt, M. (2014b). A fluorescence anisotropy-based Myt1 kinase binding assay. Assay Drug Dev. Technol. *12*, 136–144.

Santaguida, S., and Musacchio, A. (2009). The life and miracles of kinetochores. EMBO J. *28*, 2511–2531.

Shalem, O., Sanjana, N.E., Hartenian, E., Shi, X., Scott, D.A., Mikkelsen, T.S., Heckl, D., Ebert, B.L., Root, D.E., Doench, J.G., and Zhang, F. (2014). Genome-scale CRISPR-Cas9 knockout screening in human cells. Science *343*, 84–87.

Shi, J., Wang, E., Milazzo, J.P., Wang, Z., Kinney, J.B., and Vakoc, C.R. (2015). Discovery of cancer drug targets by CRISPR-Cas9 screening of protein domains. Nat. Biotechnol. *33*, 661–667.

Son, M.J., Woolard, K., Nam, D.H., Lee, J., and Fine, H.A. (2009). SSEA-1 is an enrichment marker for tumor-initiating cells in human glioblastoma. Cell Stem Cell *4*, 440–452.

Stupp, R., Mason, W.P., van den Bent, M.J., Weller, M., Fisher, B., Taphoorn, M.J., Belanger, K., Brandes, A.A., Marosi, C., Bogdahn, U., et al.; European Organisation for Research and Treatment of Cancer Brain Tumor and Radiotherapy Groups; National Cancer Institute of Canada Clinical Trials Group (2005). Radiotherapy plus concomitant and adjuvant temozolomide for glioblastoma. N. Engl. J. Med. *352*, 987–996.

Sun, T., and Hevner, R.F. (2014). Growth and folding of the mammalian cerebral cortex: from molecules to malformations. Nat. Rev. Neurosci. *15*, 217–232.

Sun, L., Shi, L., Li, W., Yu, W., Liang, J., Zhang, H., Yang, X., Wang, Y., Li, R., Yao, X., et al. (2009). JFK, a Kelch domain-containing F-box protein, links the SCF complex to p53 regulation. Proc. Natl. Acad. Sci. USA *106*, 10195–10200.

Szklarczyk, D., Franceschini, A., Wyder, S., Forslund, K., Heller, D., Huerta-Cepas, J., Simonovic, M., Roth, A., Santos, A., Tsafou, K.P., et al. (2015). STRING v10: protein-protein interaction networks, integrated over the tree of life. Nucleic Acids Res. *43*, D447–D452.

Toledo, C.M., Herman, J.A., Olsen, J.B., Ding, Y., Corrin, P., Girard, E.J., Olson, J.M., Emili, A., DeLuca, J.G., and Paddison, P.J. (2014). BuGZ is required for Bub3 stability, Bub1 kinetochore function, and chromosome alignment. Dev. Cell *28*, 282–294.

Verhaak, R.G., Hoadley, K.A., Purdom, E., Wang, V., Qi, Y., Wilkerson, M.D., Miller, C.R., Ding, L., Golub, T., Mesirov, J.P., et al.; Cancer Genome Atlas Research Network (2010). Integrated genomic analysis identifies clinically relevant subtypes of glioblastoma characterized by abnormalities in PDGFRA, IDH1, EGFR, and NF1. Cancer Cell *17*, 98–110.

Villeneuve, J., Scarpa, M., Ortega-Bellido, M., and Malhotra, V. (2013). MEK1 inactivates Myt1 to regulate Golgi membrane fragmentation and mitotic entry in mammalian cells. EMBO J. *32*, 72–85.

Wang, T., Wei, J.J., Sabatini, D.M., and Lander, E.S. (2014). Genetic screens in human cells using the CRISPR-Cas9 system. Science *343*, 80–84.

Wang, T., Birsoy, K., Hughes, N.W., Krupczak, K.M., Post, Y., Wei, J.J., Lander, E.S., and Sabatini, D.M. (2015). Identification and characterization of essential genes in the human genome. Science, Published online October 15, 2015.

Watanabe, N., Broome, M., and Hunter, T. (1995). Regulation of the human WEE1Hu CDK tyrosine 15-kinase during the cell cycle. EMBO J. *14*, 1878–1891.

Weinstein, I.B., and Joe, A. (2008). Oncogene addiction. Cancer Res. *68*, 3077–3080, discussion 3080.

Wiedenheft, B., Sternberg, S.H., and Doudna, J.A. (2012). RNA-guided genetic silencing systems in bacteria and archaea. Nature *482*, 331–338.

Wu, S.H., Bi, J.F., Cloughesy, T., Cavenee, W.K., and Mischel, P.S. (2014). Emerging function of mTORC2 as a core regulator in glioblastoma: metabolic reprogramming and drug resistance. Cancer Biol. Med. *11*, 255–263.

Wurdak, H., Zhu, S., Romero, A., Lorger, M., Watson, J., Chiang, C.Y., Zhang, J., Natu, V.S., Lairson, L.L., Walker, J.R., et al. (2010). An RNAi screen identifies TRRAP as a regulator of brain tumor-initiating cell differentiation. Cell Stem Cell *6*, 37–47.